applied sciences

MDPI

Article

Multifactorial Analysis of Wood Deterioration in Ancient Egypt: A Case Study of Khufu's Second Solar Boat

Shimaa Ibrahim [1], Paola Grenni [2,*], Lucia Mancini [3], Marco Voltolini [4], Hanan Mohamed Kamal Abdel-Fatah [5], Ahmed Refaat [6,7] and Dina M. Atwa [8]

[1] Grand Egyptian Museum, Conservation Center, Ministry of Antiquities, Museums Sector, El-Remaya Square, Giza 12561, Egypt; shimaa_sa3d53@yahoo.com
[2] National Research Council, Water Research Institute, via Salaria km 29.300, Monterotondo, 00010 Rome, Italy
[3] Department of Materials, Slovenian National Building and Civil Engineering Institute (ZAG), Dimičeva Ulica 12, 1000 Ljubljana, Slovenia; lucia.mancini@zag.si
[4] Department of Earth Sciences "Ardito Desio", University of Milan, 20133 Milano, Italy; marco.voltolini@unimi.it
[5] Department of Botany, Faculty of Science, Cairo University, Giza 12613, Egypt; hananosman@sci.cu.edu.eg
[6] Spectroscopy Department, National Research Centre, 33 El-Bohouth St., Dokki, Giza 12622, Egypt; am.refaat@nrc.sci.eg
[7] Molecular Modeling and Spectroscopy Laboratory, Centre of Excellence for Advanced Science, National Research Centre, 33 El-Bohouth St., Dokki, Giza 12622, Egypt
[8] Department of Laser Interaction with Matters, Laser Institute for Research and Applications, Beni-Suef University, Beni-Suef 62517, Egypt; dina.mohamed@lira.bsu.edu.eg
* Correspondence: paola.grenni@cnr.it

Abstract: This study presents a multi-analytical investigation of the wooden components from Khufu's Second Solar Boat, one of the valuable archaeological discoveries in ancient Egypt. The research integrates advanced imaging and analytical techniques to identify wood species, assess deterioration patterns, and characterize the fungal and bacterial biodeteriogens. The initial visual examination documented the state of preservation at the time of discovery. Subsequently, the identification of the wood species was carried out. The deterioration status was assessed using a variety of tools, including scanning electron microscopy (SEM) and high-resolution synchrotron radiation computed microtomography (SR-μCT) for morphological alterations, X-ray diffraction (XRD) for crystallinity changes and Fourier-transform infrared spectroscopy (FTIR) to assess chemical degradation indexes of wood. Moreover, molecular techniques were used to identify and characterize the presence of biodeterioration agents. Results indicate that ancient craftsmen used cedar wood for the boat construction. The analysed samples exhibited advanced biotic and abiotic degradation, as evidenced by microbiological assessments, XRD measurements of cellulose crystallinity, FTIR indices, SEM micrographs and SR-μCT data. These results provide crucial insights into the long-term degradation processes of archaeological wood in arid environments, enhancing our understanding of ancient Egyptian woodworking practices and informing future conservation strategies for similar artifacts.

Keywords: archaeological wood conservation; multi-analytical characterization; biodeterioration analysis; ancient Egyptian woodworking; X-ray microtomography; Lebanon cedar

Academic Editor: Dimitris Mossialos

Received: 17 February 2025
Revised: 27 March 2025
Accepted: 30 March 2025
Published: 3 April 2025

Citation: Ibrahim, S.; Grenni, P.; Mancini, L.; Voltolini, M.; Abdel-Fatah, H.M.K.; Refaat, A.; Atwa, D.M. Multifactorial Analysis of Wood Deterioration in Ancient Egypt: A Case Study of Khufu's Second Solar Boat. *Appl. Sci.* **2025**, *15*, 3952. https://doi.org/10.3390/app15073952

1. Introduction

In ancient Egypt, wood was essential for both practical and symbolic reasons. It was used for the construction of buildings and ships and played a significant role in religious and funerary practices. Ornate sarcophagi, ritual boats, temple doors and statues for

the deceased's spirit were made of wood, emphasising its spiritual significance. This dual functionality underlined its importance in Egyptian culture [1,2]. Among the most remarkable ancient wooden artifacts are the two solar boats of King Khufu (Cheops), discovered at the base of the Great Pyramid of Giza [3–6]. Both vessels were found carefully disassembled wooden boat, precisely stacked, with hieroglyphic inscriptions on the planks. The ancient Egyptians thought that the inscriptions helped rebuild the boats in the afterlife. The boats were designed to facilitate the pharaoh's journey through the afterlife and are unique examples of ancient Egyptian woodworking technology and maritime architecture [7–10].

The Second Solar Boat of Khufu was discovered in 1954 together with the more well-known and better-preserved Khufu's First Solar Boat, which was reconstructed and exhibited shortly after its discovery in the museum of Pyramids of Giza (Cairo, Egypt). Unlike the first one, the Second Solar Boat, due to its extremely poor state of preservation, remained in situ until recent excavations and conservation efforts [5,6]. It represents a unique opportunity to study ancient Egyptian wood in its original archaeological context, having remained relatively undisturbed for over 4500 years [11,12]. This exceptional preservation state offers valuable insights into the long-term degradation processes of archaeological wood in arid environments [13].

Wood, as an organic material, undergoes complex deterioration processes influenced by both environmental factors and biological agents [14–16]. The interaction between wood and the surrounding environment is particularly critical in archaeological contexts, where prolonged exposure to varying conditions can lead to significant physical [15,16], chemical [17–19] and biological alterations [20,21]. The cellular structure of wood, comprising primarily cellulose, hemicellulose and lignin, makes it susceptible to various degradation mechanisms [22,23]. These include physical stress from environmental fluctuations, chemical degradation from moisture and salt exposure and biological attack by microorganisms [16].

In arid archaeological environments like those of Egypt, wood deterioration follows specific patterns influenced by environmental and biological factors. Drying leads to shrinkage and splitting, while salt crystallization breaks down cellular structures. Additionally, biodeterioration by insects and microorganisms further deteriorates the integrity of wooden artifacts [24–27]. Although dry conditions generally initially inhibit biodeterioration, they are responsible for dimensional changes, cellular collapse and chemical modifications of wood components [24,25]. The presence of salts, common in desert soils, can further complicate these processes by catalysing chemical reactions and causing mechanical stress through crystallization cycles [26,27].

The characterisation of wood species and the deterioration of ancient Egyptian wooden artifacts have been extensively analysed using a combination of different tools such as microscopy, spectroscopy and microbiological evaluations, providing valuable insights into decay processes and wood preservation. XRD analyses give information about the crystallinity of cellulose and the presence of inorganic compounds, while FTIR ones reveal chemical and structural changes of decayed wood [16,28,29]. For example, wood degradation of the King Djedefre statue using XRD, FTIR and SEM was recently determined [16]. The species identification of ancient Egyptian wood by optical microscopy and the wood deterioration processes and chemical changes were performed using XRD and FTIR spectroscopy [28]. Wood characterization and preservation for polychromatic wooden coffins from the New Kingdom period were performed using multispectral imaging, optical microscopy, X-ray fluorescence (XRF) spectroscopy, visible reflectance spectroscopy (Vis-RS), Raman spectroscopy, FTIR and XRD [30]. The same multi-analytical approach was used by Vigorelli et al. [31] to evaluate an ancient Egyptian wooden statuette (representing an

offering bearer). Combined imaging and spectroscopic techniques to evaluate the degradation state and chemical changes of ancient wood (a stucco in the historic Citadel of Salah al-Din al-Ayyubi in Cairo, Egypt) were also recently used by Afifi et al. [32]. A protocol for studying highly degraded waterlogged wood anatomy using SEM was provided by Balzano et al. [33] for prehistoric pile dwellings, and new methodologies for examining highly degraded dry archaeological wood samples from Egypt using SEM and attenuated total reflectance-Fourier transform infrared (ATR-FTIR) were set up by Tamburini et al. [34]. Some semi-invasive techniques involving the destruction of pieces of wood for wood characterization have also been recently used [29]. Finally, new markers for degradation in archaeological wood were recently established, specifically focusing on characteristic changes in cellulose structure in arid environments using XRD and FTIR spectroscopy [29,35]. However, comprehensive studies integrating multiple analytical approaches remain relatively scarce, particularly those involving advanced imaging techniques and molecular biological methods [36,37].

The identification of wood species in archaeological contexts has several challenges, traditionally relying on microscopic examination of anatomical features [28]. Three-dimensional (3D) imaging technologies, particularly X-ray computed microtomography (X-μCT), have introduced new possibilities for the non-destructive identification of wood species [38]. This technique, when combined with the traditional SEM analyses, offers unique insights into wood structure and deterioration patterns at multiple scales [39,40]. In this regard, high-resolution X-μCT (e.g., synchrotron radiation computed microtomography, SR-μ-CT) to identify degraded archaeological wood species has been recently reported [41–43].

The traditional (cultivated-based) methods for biodeteriogen identification have been the most frequently used in archaeological contexts. For example, the cultivation on media and morphological identification of biodeteriogens by microscope (e.g., *Aspergillus* and *Penicillium* fungal species, known for their ability to produce cellulolytic enzymes that degrade cellulose-rich materials) and the plate assay for detecting fungal extracellular cellulase activity have been the most techniques applied [44,45].

The characterisation of biodeteriogens of archaeological wood has improved significantly with molecular techniques (e.g., polymerase chain reaction (PCR)-based analyses) [46], allowing precise identification of these microorganisms. Furthermore, high-throughput sequencing of biodeteriogens has been recently used to explore the microbial diversity and composition [46]. This information is crucial for understanding both historical degradation processes and potential ongoing biological threats to wooden artifacts. When combined with microscopic and molecular techniques, these methods offer a comprehensive understanding of degradation mechanisms and their effects on wood structure and composition [16].

Recent developments in conservation science emphasize the importance of understanding deterioration mechanisms for developing effective preservation strategies. This is particularly relevant for unique artifacts like Khufu's Second Solar Boat, where conservation decisions have to be based on thorough scientific analysis of current conditions and potential degradation risks.

The multi-analytical study presented here aimed to bridge existing knowledge gaps by implementing a comprehensive analytical approach to the study of the wooden components of Khufu's Second Solar Boat, focusing on a detailed understanding of the wood species of the boat, state of preservation and the various degradation mechanisms. This information is crucial not only for archaeological and historical interpretation but also for informing future conservation strategies for similar artifacts.

2. Materials and Methods

2.1. Historical Background and Samples' Description

In 1954, two ancient boat pits were found just south of the Great Pyramid of King Khufu, who ruled from 2589 to 2566 BCE [12,47]. The boat called the "First Boat" came from the eastern pit, and the "Second Boat", from the western one. Due to the poor state of wood preservation, the Second Boat remained sealed in its pit until 2009, unlike the First Boat, which was lifted in 1954 [12,47]. Since 2021, when the highly successful Egyptian–Japanese collaboration to assemble the Second Khufu Boat began, the stone blocks which covered the burial pit, were lifted for the first time since the reign of King Djedefre during the Old Kingdom. Similar to the First Khufu Boat lifted in 1954, the pit of the Second Boat was carefully sealed with limestone blocks, and the boat was typically dismantled into pieces, with each component carefully placed in a specific arrangement [12,47]. The boat just after lifting stone blocks is shown in Figure 1a. The poor state of preservation of the boat was evident and was confirmed by the analyses reported in this study. The alteration of the wood layers (Figure 1a, red arrow) was pronounced in the pit, which decreased as a result of the loss of wood properties. The first wooden bar lifted, approximately 1 metre long, is shown in Figure 1b. A large-scale conservation and reconstruction project of the Second Boat is currently in progress. A key first step in conservation was to identify the types of wood used by the ancient builder, assess the boat's state of decay and determine the best conservation methods. The boat consisted of various parts, including the deckhouse, canopy, forecastle, deck beam, hull, ribs and oars [48,49].

Figure 1. Pictures of some wood parts of the King Khufu (Cheops) Solar Boat. (**a**): The state of the boat just after lifting the stone blocks; the red arrows point to the wood height change marks resulting from 4500 years of buried time. (**b**): The first bar of wood after lifting the pit (about 1 m long); blue arrows indicate the variation of wood colour along the bar, while the red one indicates the surficial normal wood cavities.

The present work focuses in particular on the types of wood used in the construction of the deckhouse, canopy and bow castle. For this purpose, three small samples were collected, one from each of the specified parts (referred to as sample 1, 2 and 3). The shape of the samples was semi-cylindrical, with a diameter of 5–7 mm and a height of approximately 10 mm.

2.2. Wood Identification

For the identification of wood species, synchrotron radiation computed microtomography (SR-μ-CT) measurements were performed at the SYRMEP (SYnchrotron Radiation for MEdical Physics) beamline of the Elettra synchrotron facility in Basovizza (Trieste, Italy) [50]. The measurements were performed in the polychromatic beam configuration

using a multiscale approach. The white beam was pre-filtered using 1.0 mm of silicon plus 0.025 mm of molybdenum, corresponding to an average beam energy of ca. 20 keV. The detector comprised a water-cooled 16-bit macroscope sCMOS camera (2048 × 2048 pixels) lens coupled with a GGG scintillator screen. Two different pixel sizes were used for the tomographic image acquisition: 0.9 μm (corresponding to a field of view of ca. 1.8 × 1.8 mm^2) and 2.4 μm (corresponding to a field of view of ca. 4.9 × 4.9 mm^2).

In order to enhance edge detection and interface visualization between phases with similar X-ray attenuation coefficients, the images were acquired in propagation-based phase-contrast mode [51] by setting up a sample-to-detector distance equal to 100 mm. Prior to μCT scans, samples were embedded in thin Parafilm foils to ensure a constant moisture content and a consequent stability in the X-ray beam. The sample radiographs (projections) were collected by rotating each specimen over 180 degrees with an exposure time per projection of 150 ms. In total, each μCT scan comprised 1800 sample projections. In some cases, we focused on specific regions of interest (ROIs), while in other cases, we used the vertical stack modality, moving the sample vertically in the X-ray beam and then stitching contiguous volumes.

Tomographic reconstruction, including single-distance phase recovery (Paganin's algorithm [52]) of projections and removal of annular artifacts, was performed using the SYRMEP Tomo Project software suite (STP, developed at Elettra synchrotron facility), using Paganin's phase recovery algorithms. The phase recovery algorithm reveals important information from contrast images, improving the visibility of microstructures in organic materials and preserving spatial resolution. The removal of annular artifacts eliminates detector-induced patterns that could mask critical degradation features. Together, these methods enable non-destructive visualisation of patterns of deterioration at the cellular level that would be undetectable with conventional tomographic techniques, providing conservators with valuable microstructural information without damaging samples [53].

The 2D virtual sections of the reconstructed volumes were visualized using the open-source software ImageJ Fiji [54], while for the volumetric visualization, by a 3D rendering procedure, the commercial VGStudio 2.0 software (Volume Graphics, GmbH, Heidelberg, Germany) was used.

Wooden sections were also examined using a light microscope (Axio Imager M2, Zeiss, Microimaging GmbH, Göttingen, Germany) equipped with a digital camera. Images were acquired and processed by Zen 2.3 Pro (Zeiss) to confirm identification of wood species [53].

2.3. Physical and Chemical Wood Degradation

To evaluate the physical and chemical degradations of the boat wood, a set of diagnostic techniques were used, including SEM for identifying the wood surface morphology, as well as XRD and FTIR to trace the chemical changes occurred [16,28,55].

2.3.1. SEM Analyses

Morphological characterization of the degraded wooden specimens was performed using a SEM-Quanta FEG-250 environmental scanning electron microscope (FEI Co., Hillsboro, OR, USA) equipped with an energy dispersive X-ray (EDX) spectroscopy unit. Specimens were examined under high vacuum conditions without prior preparation. Micrographs were acquired using a backscattered electrons detector (BSED) with a spatial resolution of 1.4 nm at an accelerating voltage of 20 kV. EDX analysis was conducted to determine the elemental composition at specific regions of interest [16].

2.3.2. XRD Analyses

X-ray diffraction analysis was conducted at the MCX beamline of the Elettra-Sincrotron Trieste Research Centre to evaluate the cellulose crystallinity index (CrI) as a measure of

wood degradation [56,57]. The wood samples were pulverized using an agate mortar and analysed at room temperature using a capillary spinner sample holder. The experimental setup comprised a 4-circle Huber diffractometer with a 3D translation stage, equipped with a high-count rate fast scintillator detector. The detector configuration included two slits with vertical apertures of 200 and 300 μm, positioned 90 cm from the sample. Diffraction patterns were acquired using a monochromatic beam with the following parameters: energy = 12 keV, acceleration current = 158.84 mA and X-ray wavelength = 1.0332 Å. Sample alignment was achieved using a laser interferometer, with measurements conducted at a fixed incident angle of 4 degrees. Data collection was performed in transmission mode across the angular range from 4° to 70° to identify cellulose crystallinity index and the range from 4° to 30°; other interfering compounds were observed in the remaining ranges. Data analysis was performed using the PDF4 software.

The degradation degree was quantified through cellulose crystallinity measurements using the widely adopted Segal method. The crystallinity index (CrI%) was calculated according to the following equation:

$$CrI\% = [(I_{200} - I_{am})/I_{200}] \times 100$$

where I_{200} represents the intensity of the (200) peak, corresponding to both crystalline and amorphous phases, and I_{am} denotes the intensity minimum between the (200) and (101) peaks, with the (101) peak representing amorphous cellulosic fibres [58,59].

2.3.3. FTIR Analyses

Attenuated total reflection (ATR) FTIR spectra were obtained using the ALPHA II FTIR spectrometer (Bruker Optik GmbH, Ettlingen, Germany) in the spectral range of 4000–400 cm^{-1} with a resolution of 4 cm^{-1}.

Some FTIR indices were calculated according to previous studies for quantitative analysis and to assess wood degradation in archaeological or aged wood samples [59–66]. The lignin index was estimated by the ratio between the absorption intensities at ~1592 cm^{-1} and ~1505 cm^{-1}, where the lower values indicate lignin degradation. The carbohydrates/lignin index was estimated by the ratio between the absorption intensities at ~1735 cm^{-1} for carbohydrates and ~1505 cm^{-1} for lignin. An increase in this ratio indicates lignin degradation relative to carbohydrates. Crystallinity index (CrI) was estimated by the ratio between the bands at ~1375 cm^{-1} and ~2900 cm^{-1}, which indicates the relative proportion of crystalline vs. amorphous cellulose, where the higher values suggest the degradation of amorphous regions [67]. The peak intensities were calculated relative to the baselines properly constructed for each peak.

2.4. Evaluation of Biodeteriogens

2.4.1. Isolation of Deteriorating Fungi

Deteriorating fungal species were isolated from the wooden archaeological objects by swabbing from the deteriorated surface of the wooden objects (10 swabs) and by serial dilutions of the broken deteriorated parts from sample (5 samples). Each sampling was performed in five replicates. Isolation was performed using two types of media: Carboxy methyl cellulose agar (CMC) and wood straw agar media. CMC was prepared dissolving in 1 L: Carboxy methyl cellulose 10 g, NH_4 Cl 1 g, KNO_3 1 g, $MgSO_4 \times 7H_2O$ 0.5 g, KH_2PO_4 1 g, Agar 20 g. Wood straw agar medium was prepared dissolving in 1 L: wood straw 10 g, NH_4Cl 1 g, KNO_3 1 g, $MgSo_4 \times 7H_2O$ 0.5 g, KH_2PO_4 1 g, Agar 20 g. Inoculated plates were incubated at 30 °C for 7 days [44,55]. Cultures were purified by sub-culturing several times until pure isolates were obtained and preserved on potato dextrose agar slants.

2.4.2. Morphological Identification of Deteriorating Fungal Isolates

For the identification of fungi at the species level, isolates were inoculated on the Czapek-Dox agar medium and malt extract agar medium. Macroscopic characteristics (colour, texture appearance and diameter of the colonies) and microscopic (microstructures) were examined by a light microscope (Axio Imager.A2, Carl Zeiss, Oberkochen, Germany, 100× magnification). Fungal isolates were identified according to previous studies [68–77].

2.4.3. Identification of the Highly Frequent Fungal Species by Molecular Methods

Fungal isolates with cellulose activity (evaluated by the Congo red plate-based test [78]) were selected for molecular identification. The isolates were cultured in Czapek-Dox broth at 30 °C for 5 days, and the fungal mycelium was filtered and ground into fine powder using liquid nitrogen. DNA extraction was performed with the Quick DNA Fungal Microprep Kit (Sigma-Aldrich), and PCR was carried out using Maxima Hot Start PCR Master Mix (Thermo K1051, Sigma Aldrich, St. Louis, MO, USA) and ITS1/ITS4 primers. The reaction (50 µL) contained 25 µL of Master Mix (2×), 5 µL of template DNA, 18 µL of nuclease-free water and 1 µL (20 µM) of each primer. Thermal cycling included initial denaturation at 95 °C for 10 min, followed by 35 cycles: 30 s at 95 °C, 1 min at 57 °C and 90 s at 72 °C, with a final extension at 72 °C for 10 min. PCR products were purified using the GeneJET PCR Purification Kit (Thermo Scientific, Waltham, MA, USA) and sequenced by GATC Biotech (Ebersberg, Germany) on an ABI 3730XL DNA sequencer (Applied Biosystems, Foster City, CA, USA). Sequences were aligned according to established protocols [79], compared with GenBank reference sequences, and a phylogenetic tree was generated using MEGA 11 software.

3. Results and Discussion

3.1. Wood Species Identification

The internal anatomical structure of the tested sample examined by SR-µ-CT are visible in Figure 2a. The images revealed the presence of soil particles. The anatomical characteristics are consistent with *Cedrus libani* taxonomy. In fact, distinctive growth ring formations with clear transitional boundaries and periodic patterns, which are characteristic of Mediterranean cedar species, were observed. The cellular architecture displayed systematic tracheid arrangements typical of gymnosperm wood anatomy, with dimensions and organizational patterns specifically concordant with *C. libani* morphology. Notable anatomical features include well-defined ray structures, resin canal formations and degradation patterns consistent with archaeological wood specimens [80]. This identification aligns with previous historical evidence of extensive cedar importation from Lebanon during the Old Kingdom period, particularly for elite shipbuilding projects, due to its superior mechanical properties including enhanced durability and hydrophobic characteristics [47,81,82]. The presence of *C. libani* in this royal naval architecture exemplifies the sophisticated material selection practices employed in ancient Egyptian manufacturing processes.

These results were confirmed by both the SEM images (Figure 2b) and the light microscope analyses (Figure 3). In particular, SEM analyses highlighted degraded parts of the wood, soil residues and wood tissue separations.

The micromorphological features of the wooden sections, observed under a light microscope (Figure 3), highlighted the presence of a distinct cellular arrangement, including tracheids, ray parenchyma and resin canals, which are characteristic of *Cedrus libani* in the transverse section (Figure 3a). Additionally, the radial section exhibited longitudinal tracheids with bordered pits (Figure 3b,c) [28,47].

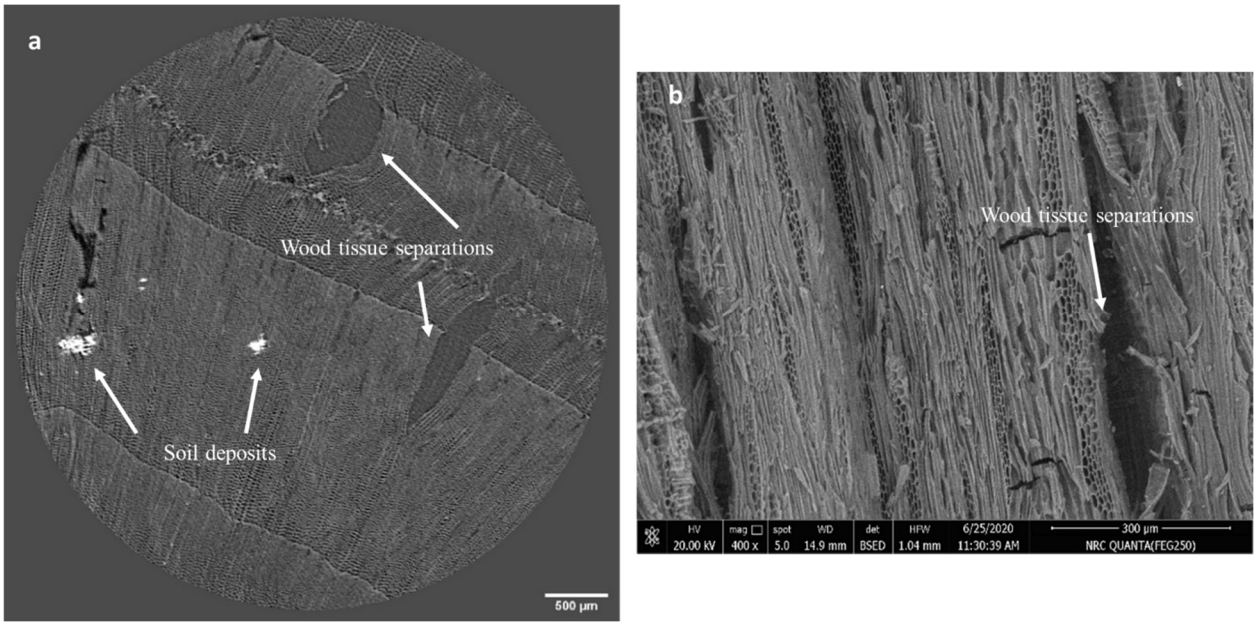

Figure 2. Images of the tested wooden samples. (**a**): Synchrotron-based X-ray microtomography (SR-µ-CT) virtual section (isotropic voxel size = 2.4 µm); the anatomical pattern of wood is visible. The arrows highlight some degradation evidences in the form of separations on the wood texture and the interferences with soil particulates. (**b**): A SEM image of the wood sample. Arrows highlight the wood tissue separations and soil deposits.

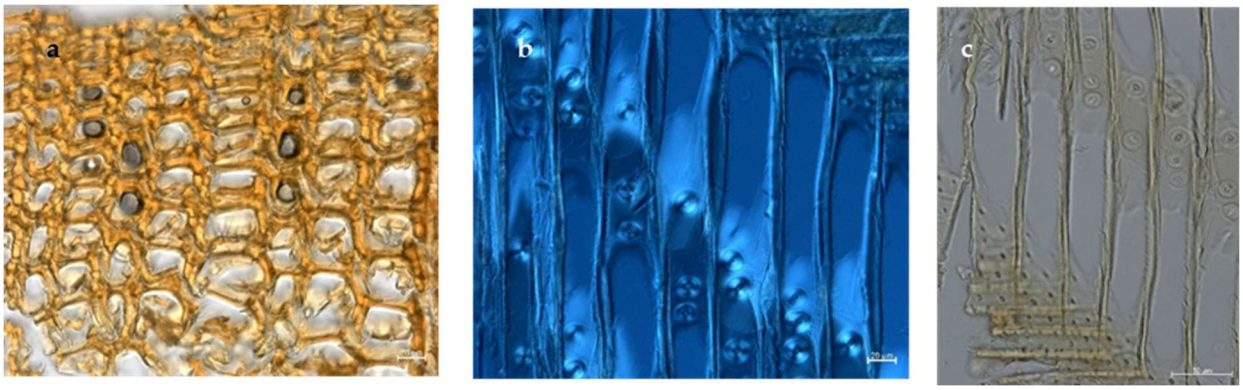

Figure 3. Pictures of wooden sections, observed under a light microscope, for the observation of the micromorphological features. (**a**): Transverse section showing the cellular arrangement, including tracheids, ray parenchyma and resin canals characteristic of *Cedrus libani*. (**b**,**c**): Radial sections of the wood sample. (**b**) Axial tracheid pits with scalloped tori, along with the presence of ray tracheids. C: Longitudinal tracheids with bordered pits. The observed anatomical features, including tracheid structure and pitting patterns, are consistent with *Cedrus libani* identification. Scale bars: a and b = 20 µm; c = 50 µm.

3.2. Physical and Chemical Degradation

3.2.1. Results of SEM Analysis

The identification of the plant species (*Cedrus libani*), carried out by SR-µ-CT, was confirmed by SEM micrographs (Figure 4c–e), which also showed different mechanisms of deterioration of the ultrastructure of the wood. SEM images can reveal how the physical and chemical properties of wood undergo a significant transformation as a result of degradation over time. Overall, the extensive cell collapse visible in the images shows how these degradation processes gradually disrupted the internal structure of the wood, leading to significant changes in its material properties. Anatomical features showed diagnostic characteristics, including the systematic arrangement of tracheids, distinctive

pit formations in the radial walls and a species-specific radial morphology (Figure 4c). The deterioration assessment indicated significant structural modifications manifesting in several pathological phenomena: physical degradation evidenced by cellular deformation, tracheid wall fracturing, middle lamella deterioration and partial structural collapse. Biochemical deterioration was demonstrated by cell wall thinning, irregular erosion patterns indicative of microbial activity and material loss in highly degraded regions, accompanied by apparent mineral depositions visible as electron-dense regions (Figure 4d,e) [83,84].

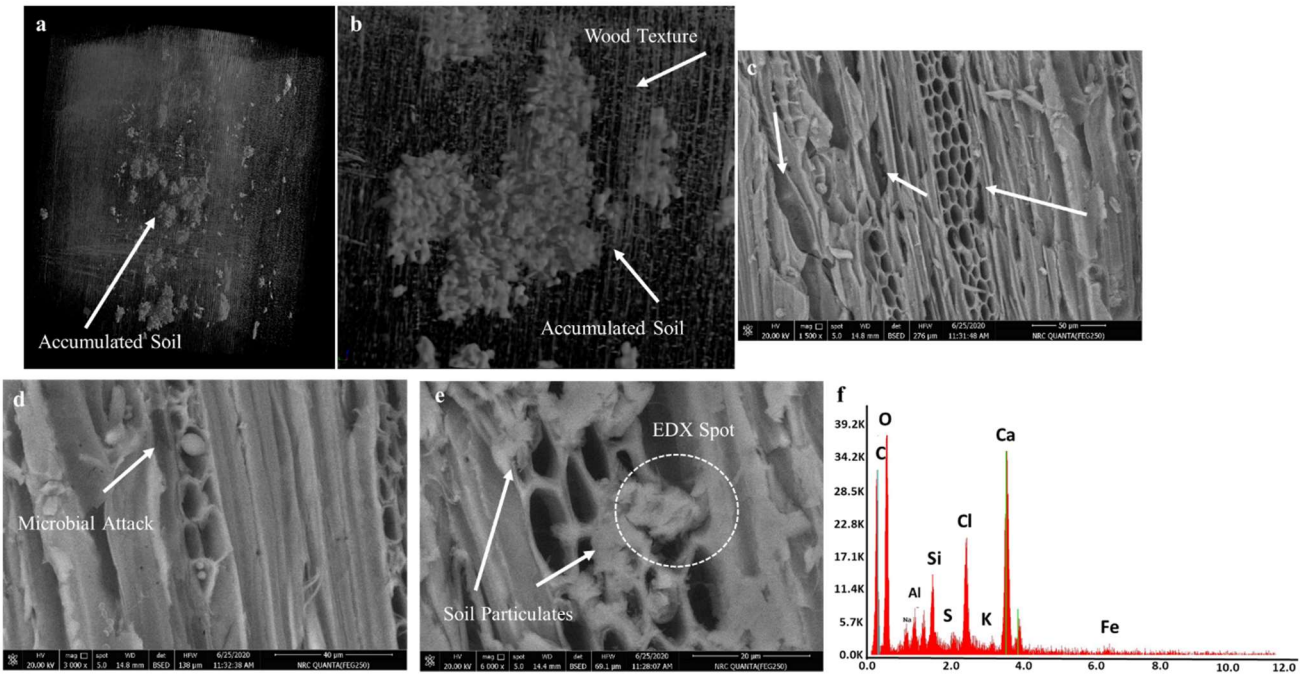

Figure 4. (**a**): 3D rendering of a sub-volume obtained by SR-μ-CT measurements (isotropic voxel size = 2.4 μm), and (**b**): zoomed region of this volume showing the details of interest: soil particles inside the wood sample are evident; the shape of soil deposits and the wood anatomical structure are also visible. (**c**–**e**): SEM micrographs. Different degradation signs of the wood samples (cellular deformation, tracheid wall fracturing, middle lamella deterioration and partial structural collapse in addition to microbiological attacks) are indicated by white arrows. In panel e, soil particulates are indicated at the point of energy-dispersive X-ray spectroscopy (EDX) analysis. (**f**): EDX analysis. Ca (as the indication of calcite and gypsum, the main compositions of the burial pit, Calcite Champer), Si (as the indication for SiO_2 from the sealing mortar of covering blocks), C and O were the main wood constituents. Small amounts of Al, Mg and Na were also detected as soil-derived components.

The structural alterations included weakened intercellular adhesion, cell wall separation, anatomical distortion and void formation through material loss.

From a physical point of view, the progressive cellular structure breakdown leads to a reduction in strength, an increase in porosity, a decrease in density and an increase in brittleness, ultimately altering the mechanical properties of wood [28,80]. Chemically, wood undergoes complex molecular transformations with the breakdown of lignin and cellulose. This leads to changes in its chemical composition, surface chemistry and molecular reactivity [85,86]. These microscopic changes are the result of complex interactions, including enzymatic degradation by microorganisms, oxidative reactions, the hydrolysis of chemical bonds and environmental factors such as temperature and humidity [87].

The 3D rendering obtained by SR-μCT data revealed a soil particle accumulation within the wood matrix (Figure 4a). The zoomed region in Figure 4b distinctly delineates soil deposits while simultaneously illustrating the wood anatomical architecture in the 3D domain.

Overall, the 3D SR-μCT images and SEM micrographs revealed that the soil-induced wood decay was a complex, multifactorial process in which soil deposits played the role of catalysts for mechanical, chemical and biological breakdown. Indeed, soil particles are known to apply mechanical stresses to wood structures, inducing chemical changes and creating microenvironments that promote microbial decomposition. By infiltrating cellular spaces and simultaneously triggering multiple degradation mechanisms, these deposits significantly compromised the integrity of the wood, accelerating its natural decomposition [88].

EDX analysis showed the presence of specific elements that played distinct roles in the deterioration processes (Figure 4e,f). Calcium (Ca) indicates the deposition of calcite from the burial chamber, forming crystalline deposits within the wood cells that exerted mechanical stress through crystal growth. Gypsum, a degraded form of calcite, was confirmed by the presence of sulphur (S), which accelerated the breakdown of cellulose through mild acidification, forming hygroscopic compounds that attracted moisture and created physical stress through hydration/dehydration cycles. Silicon (Si), probably due to SiO_2 contamination of the sealing mortar, led to the formation of silicate complexes that penetrated the wood components, altering their physical properties. Overall, these mineral intrusions had a significant impact on the mechanical properties, chemical stability, porosity and long-term preservation potential of the wood, creating a complex degradation environment [89,90]. The detection of carbon (C) and oxygen (O) corresponded to the wood's organic matrix, while trace elements including aluminium (Al), magnesium (Mg) and sodium (Na), are attributed to soil-derived minerals [12,91,92].

3.2.2. FTIR Spectral Characterization and FTIR Indices

The detailed FTIR band assignments are listed in Table 1. The assignments were performed in line with previous works [93–100]. The 3500–500 cm^{-1} spectral region of the FTIR spectra of the ancient wood sample is displayed in Figure 5a.

Table 1. FTIR band assignment of the wood samples.

FTIR Band (cm^{-1})	Band Assignment
3337	O-H stretching of intermolecular hydrogen bonds
2979	Asymmetric CH stretch of the methoxy group of lignin
2943	Asymmetric CH stretching of CH_2 groups of lignin, cellulose, hemicellulose
2914	Symmetric CH stretching of CH_3 groups of lignin, cellulose, hemicellulose
1726	C=O stretching of acetyl and carbonyl groups in hemicelluloses
1590	Skeletal vibrations of the aromatic ring, together with C=O stretch in lignin
1508	C=C skeletal vibrations of the aromatic ring in lignin
1448	Aromatic C-H deformation in lignin and carbohydrates
1429	C-H in-plane deformation in lignin and carbohydrates
1376	CH bending in cellulose, hemicellulose and lignin
1264	Aromatic C-O stretching vibrations of methoxyl and phenyl propane guaiacol ring units of lignin
1233	Stretching vibrations of C-O in Xylene and syringyl ring
1157	Asymmetric bridge C-O-C stretch mode in carbohydrates
1108	Asymmetric in-plane aromatic skeletal stretching, C-C and C-O stretching
1054	C-O stretching
1029	Aromatic C-H in-plane deformation, and C-O deformation in primary alcohols
898	Aromatic C-H out-of-plane ring deformations of cellulose
851	Ring vibrations

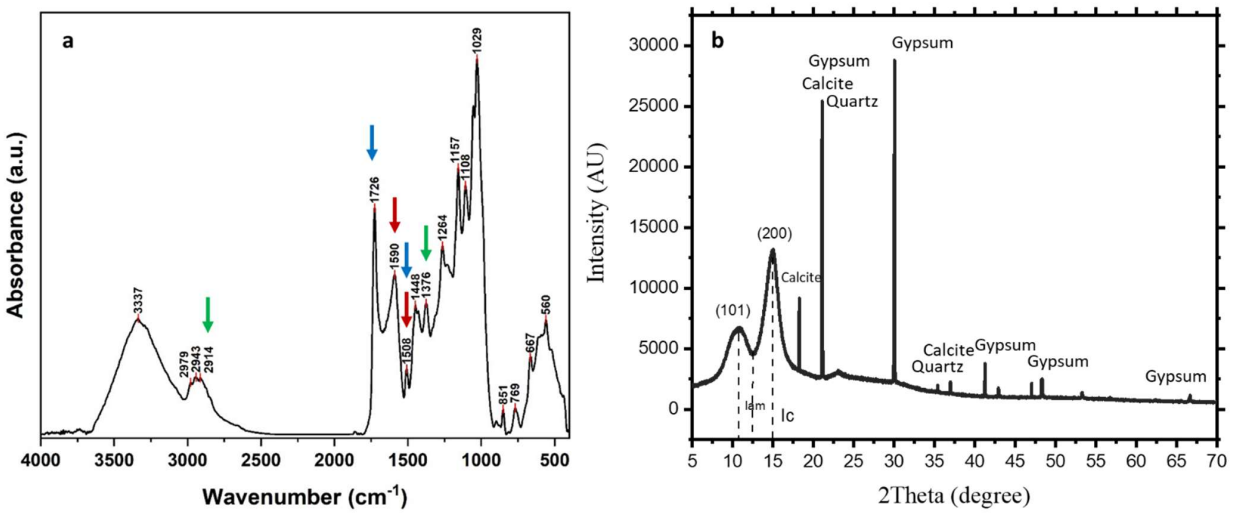

Figure 5. (**a**): FTIR spectra of the ancient wood. Red arrows indicate the characteristic bands for the lignin index (1590 cm^{-1} and 1508 cm^{-1}). Blue arrows indicate the characteristic bands for the carbohydrate/lignin index (1726 cm^{-1} and 1508 cm^{-1}), while green arrows point to the bands of cellulose crystallinity index (1376 cm^{-1} and 2914 cm^{-1}, see also Table 2). (**b**): XRD pattern of the wood sample. Soil particulates clearly appeared since they were mainly composed of calcite, gypsum and quartz in addition to the main beaks crystalline and amorphous cellulose at 2θ = 15° and 2θ = 13°, respectively.

Table 2. FTIR indices of the ancient wood samples calculated by selected FTIR absorption bands.

Index	Index	Value
Lignin Index	I_{1590}/I_{1508}	4.040
Carbohydrates/Lignin Index	I_{1726}/I_{1508}	7.656
Crystallinity Index of Cellulose Bands	I_{1376}/I_{2914}	1.019

The FTIR indices for lignin, carbohydrates/lignin and Crystallinity (Table 2) were calculated on the basis of six absorption bands (Table 1). Specifically, the intensities of lignin peaks at ~1590 cm^{-1} and ~1508 cm^{-1} were chosen as lignin references as they are due to the aromatic skeletal vibration (C=C) in lignin [64].

Moreover, the band at ~1730–1700 cm^{-1} was chosen as a reference for carbohydrate, as it possesses no contribution from lignin.

The lignin index (I_{1596}/I_{1505}) provides information on the molecular structure of aromatic lignin, while the carbohydrate/lignin index indicates the state of preservation of the carbohydrate content of wood [101]. The crystallinity index of wood cellulose in the sample was determined by calculating the I_{1376}/I_{2914} ratio [67]. This index is particularly useful for understanding structural changes in lignin, especially in archaeological wood. An increase in this ratio suggests the oxidation of aromatic lignins, the loss of guaiacyl units or, more likely, the demethoxylation of guaiacyl units [96,102]. Since lignin index refers to the extent of possible oxidation of aromatic lignin and formation of free phenol groups [88,96], it is therefore useful in revealing the state of ancient wood as some of the degradation products in aged lignin, such catechols, can result from fungal degradation [88,96].

In the present work, among the different indexes, the lignin one was the highest in the examined sample (Table 2), indicating selective decomposition within the wood's lignin structure. This suggests the oxidative breakdown of lignin aromatic rings rather than complete lignin loss, leading to increased brittleness and reduced structural integrity [102]. Moreover, the lignin index value (4.040) is comparable to those of fresh wood standard (~1.5–2.0) [103]. The high lignin index found in this work suggests a relative enrichment of lignin content. This is indeed common in archaeological wood because cellulose and

hemicellulose tend to degrade more readily than lignin, leaving behind a higher proportion of lignin in the remaining wood structure [88,96,104].

The carbohydrate/lignin index (given by the I_{1726}/I_{1508} ratio) revealed that the carbohydrate content represented by hemicellulose was very high in the sample, indicating a high content in hemicellulose with the lowest preserved lignin content [66,102]. The lower carbohydrate/lignin ratio of the sample (7.656) compared to the fresh wood standard (~8.5–10.0) [103] further confirmed the degradation pattern. This indicates a loss of carbohydrates (cellulose and hemicellulose) relative to lignin, which is a classic signature of wood degradation over time [85,104].

The lower crystallinity index (1.019) compared to fresh wood standard (~1.5–1.8) [103] suggests a degradation of the crystalline cellulose structure. This is typical in archaeological wood as the more organized crystalline regions of cellulose break down over time [85,103].

FTIR indices provided a detailed chemical analysis of wood degradation, revealing a complex process characterized by selective molecular breakdown. Overall, these results suggests a moderate to significant degradation, which is characterized by the selective loss of carbohydrates (cellulose and hemicellulose), relative enrichment of lignin content and breakdown of crystalline cellulose structures. The results show high hemicellulose content with relatively low conserved lignin, accompanied by lignin enrichment due to preferential degradation of cellulose and hemicellulose. The decrease in the carbohydrate-to-lignin ratio and reduction in crystallinity index indicate ongoing structural disorganization as the more ordered crystalline regions of cellulose degrade over time. This chemical fingerprint suggests a moderate to significant degradation pattern in which lignin remains relatively stable while carbohydrate structures gradually disintegrate.

These results provide valuable insights into the state of wood preservation and long-term molecular changes. Such molecular disintegration leaded to reduced mechanical strength, increased brittleness and alterations in porosity and dimensional stability [85,101,102,104].

3.2.3. XRD Results

The Synchrotron radiation X-ray diffraction (SR-XRD) analysis of the wood sample are shown in Figure 5b. The results revealed significant soil deposits that interfered the wood's structural composition, reflecting the extent to which the burial environment influenced the degradation stage of the boat. The XRD pattern, also supported by energy-dispersive X-ray spectroscopy (EDX) data, demonstrated the presence of calcite, gypsum and quartz—primary constituents of the burial chamber environment. XRD and EDX analyses revealed a complex degradation process driven by the mineral composition of the burial environment, with calcite, gypsum and quartz acting as key agents in wood deterioration. These mineral deposits physically alter the cellular structure of wood, trigger chemical reactions and alter internal conditions, thus creating multiple pathways of degradation. By occupying cellular spaces, altering internal pH, promoting moisture retention and catalysing oxidative processes, these minerals in the burial environment significantly transformed the physical and chemical properties of wood [88–90].

The moderate-intensity peak (012) of calcite at about 15.4° 2θ and the high-intensity peak (121) of gypsum at about 13.1° 2θ significantly overlapped with the characteristic cellulose peaks at 15.0°, 12.5° and 10.5° 2θ. Where the (200) lattice plane at 15.0° 2θ represents a critical structural feature encompassing both crystalline and amorphous phases, 12.5°2θ represents the intensity minimum between the (200) and (101) planes, demonstrating the transitional structural characteristics, and the (101) lattice plane at 10.5° 2θ represents the amorphous cellulosic fibres [28,58,59]. Therefore, the mentioned interference in the diffraction pattern hinders the accurate determination of the cellulose crystallinity index (CrI) in the composite sample when using the Segal method for quantitative analysis [105].

Consequently, the CrI measurement was performed on another pure ancient wood sample collected from the same source, yielding a CrI value of 13%. This low value indicates substantial degradation of the crystalline cellulose regions, which aligns with the Fourier-transform infrared spectroscopy (FTIR) results, demonstrating how mineral components systematically degraded the wood's molecular integrity [85,89]. The findings revealed that the burial environment was not a passive factor but an active participant in wood degradation, with mineral deposits acting as key catalysts that progressively dismantled the wood's structural and molecular composition [88–90]. The observed shift in diffraction peak positions occurred because synchrotron radiation SR- X-rays have higher energy and shorter wavelengths than conventional laboratory X-ray sources. According to Bragg's Law, shorter wavelengths produce smaller diffraction angles (2θ) for the same crystal planes. The superior monochromaticity, brilliance and collimation of synchrotron radiation also contributed to this systematic peak shift, requiring appropriate calibration when comparing diffraction patterns obtained from different X-ray sources [106,107].

3.3. Deteriorating Fungi

The 14 fungal species isolated from the deteriorated wooden objects and identified by morphological characteristics are listed in Table 3. Eight species belonged to the *Aspergillus* genera and six species belonged to *Penicillium* one. The most frequently deterioration-causing fungi species found in the current study were *Aspergillus flavus* and *A. terreus*, in line with previous studies. For example, Ahmad et al. [108] isolated *A. flavus* and *A. terreus* (together with *A. fumigatus*, *A. niger*, and *P. chrysogenum*) from a Nabataean wooden coffin, Jordon. *Aspergillus* spp. and *Penicillium* spp. were the most dominant genera isolated from the storage area of Cheops's Solar Boat and wooden frames of the Stucco window in the Islamic Art Museum [109]. *Aspergillus flavus* and *A. terreus* together with other fungal species (*A. fumigatus*, *A. niger*, *Cladosporium cladosporioides*, *Fusarium oxysporum* and *Trichoderma longibrachiatum*) were isolated by Abdel-Azeem et al. [24] from 35 archaeological pharaonic wooden artifacts. Helmi et al. [110] isolated *A. flavus* and *A. niger* from ancient funeral masks in Saqqara, Egypt, which revealed various deterioration aspects (discoloration, cracks and stains). Finally, twenty-six fungal species from the wooden objects were isolated and identified by Geweely et al. [37], and the four most frequent species belonged to the genus *Aspergillus*.

Table 3. Total counts, relative density (%) and frequency of occurrence of fungal species isolated from King Khufu's Second Boat. In bold the sum of the fungal species for each genera.

Fungal Species	Total Count	Relative Density %
Aspergillus clavatus	6	3.84
Aspergillus flavus	34	21.79
Aspergillus fumigatus	12	7.69
Aspergillus niger	15	9.61
Aspergillus ochraceus	4	2.56
Aspergillus parasiticus	8	5.12
Aspergillus terreus	24	15.38
Aspergillus versicolor	3	1.92
Total Aspergillus spp.	**106**	**67.95**
Penicillium citrinum	13	8.33
Penicillium chrysogenum	10	6.41
Penicillium glabrum	5	3.20
Penicillium multicolor	6	3.84
Penicillium capsulatum	7	4.48
Penicillium oxalicum	9	5.76
Total Penicillium spp.	**50**	**32.05**
Total count	**156**	

Identification of the Selected Deteriorating Fungal Isolates by Metagenomic Analyses

The isolate belonging to the *Aspergillus flavus* and the other isolate belonging to the *Aspergillus terreus* with the highest cellulose activity were identified using molecular biology methods based on ITS1 and ITS4 region sequences. Sequences of PCR products were aligned with the reference sequences on GenBank, identified and deposited with accession numbers on NCBI. Their identification was confirmed to be *Aspergillus flavus* (accession number PQ226812) and *Aspergillus terreus* (accession number PQ227217). Their phylogenetic Neighbour Joining (NJ) trees are shown in Figures 6 and 7. The closely related species were found using the p-distance model with the Molecular Evolutionary Genetics Analysis (MEGA) software version11 [111].

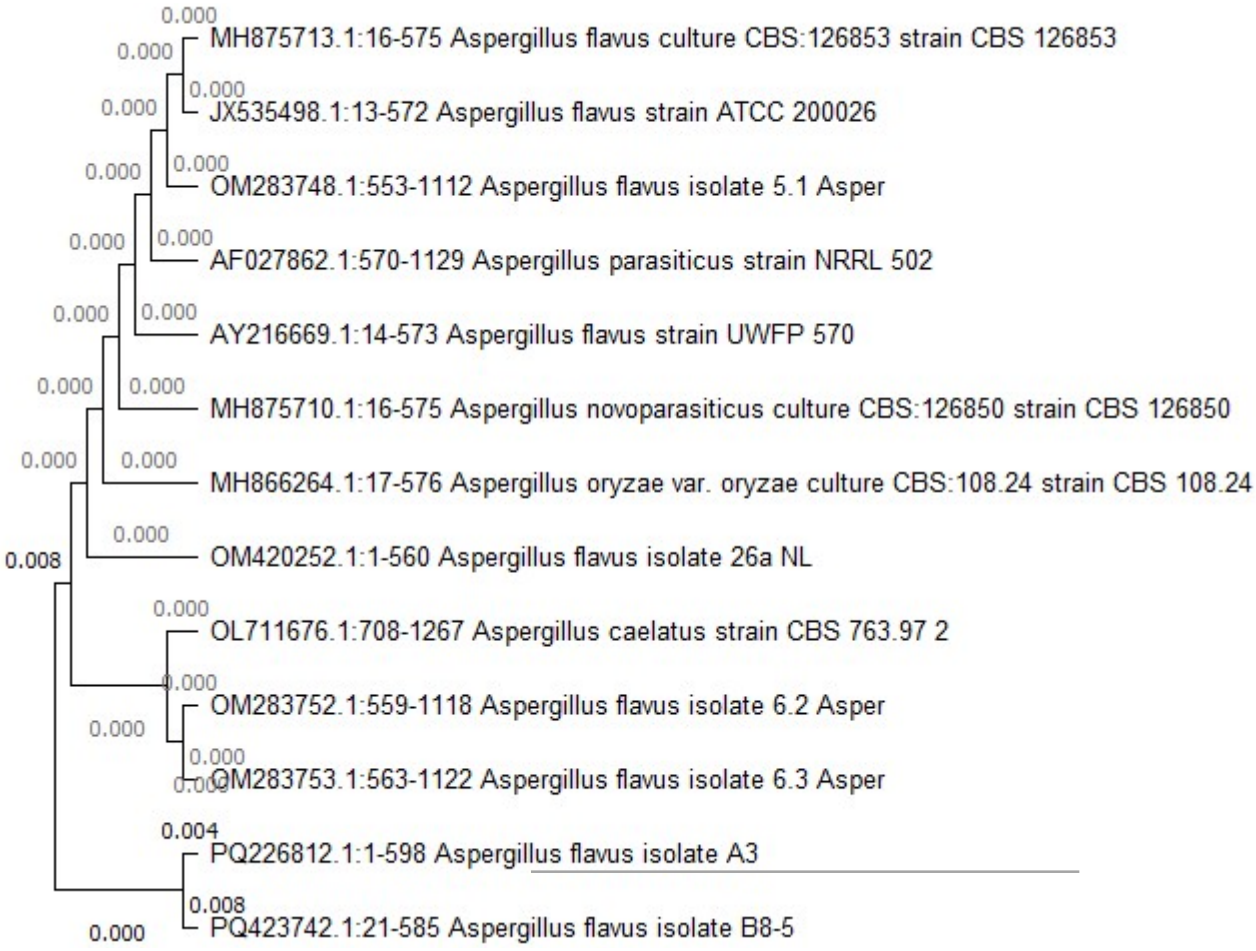

Figure 6. Neighbour joining (NJ) phylogenetic tree of *Aspergillus flavus* A3 PQ226812 based on ITS1 and ITS4 sequence, with the phylogenetic position and the closely related species.

The results found here are in line previous studies. For example, Ortiz-Santana et al. [112] isolated and identified morphologically and molecularly different species of white, brown and soft rot fungi in the structural woods of eight historical churches in Chiloé, Chile, causing decay in these historical buildings. Pedersen et al. [113] also isolated several species of *Ascomycota* soft rot and *Basidiomycota* fungi that attacked wood, leaving a weak and vulnerable wood structure. Two types of fungal degradation (brown rot and soft rot) were observed on archaeological objects in the Museum of Fine Arts, Boston and the Metropolitan Museum, New York [114].

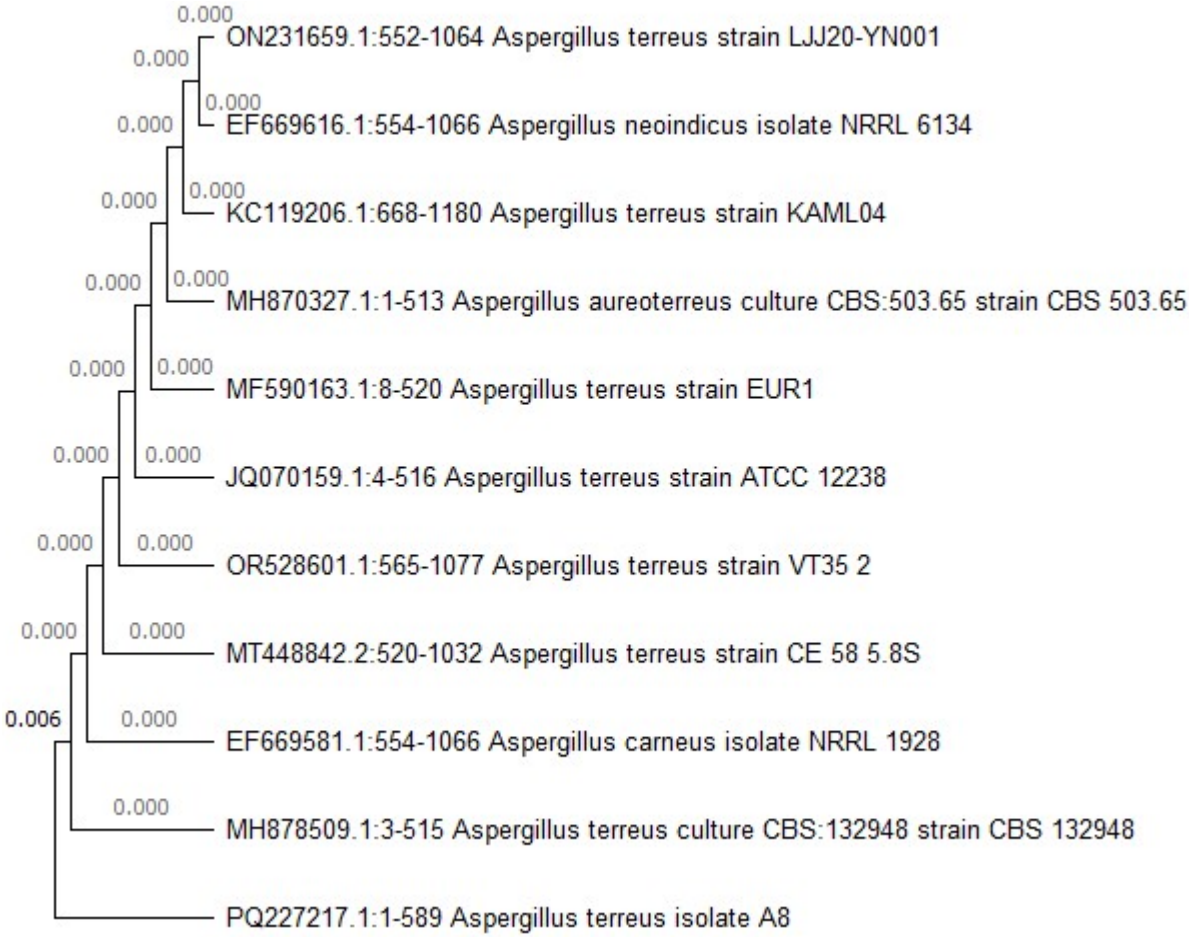

Figure 7. Neighbour joining (NJ) phylogenetic tree of *Aspergillus terreus* A8 PQ227217 based on ITS1 and ITS4 sequence, with the phylogenetic position and the closely related species.

Biological attacks on wood, particularly by fungi, involve complex enzymatic processes that contribute to oxidative degradation and hydrolysis of chemical bonds. Fungi, for example, use enzymes active on carbohydrates (CAZymes) and reactive oxygen species (ROS), such as hydrogen peroxide (H_2O_2), to degrade lignocellulose, a key component of wood decay. This enzymatic activity not only accelerates the degradation of wood components but also induces oxidative changes in the proteins involved in these processes. Fungal species isolated from wood artifacts are significant because they play a direct role in these degradation mechanisms, providing valuable insights into how biological factors contribute to structural and chemical changes in wood over time [87].

4. Implications for Egyptian Woodworking and Conservation Practices

The identification of *Cedrus libani* in this study provides empirical evidence of the strategic utilization of durable timber by Old Kingdom Egyptian craftsmen. Their knowledge of wood properties—including dimensional stability, resistance to biological degradation and mechanical strength—demonstrates an advanced understanding of material science and its application in construction and preservation.

The taxonomic identification of *Aspergillus flavus* and *A. terreus* as dominant biodeterioration agents highlights the impact of biological factors on the structural and chemical degradation of wood over time. To mitigate this, conservators should prioritize eco-friendly disinfection methods over traditional biocides, which may accelerate deterioration.

A multi-analytical approach utilizing synchrotron radiation micro-computed tomography (SR-μCT) at 0.65 μm spatial resolution enabled the non-destructive three-dimensional

visualization and quantification of internal structural changes with statistically significant reproducibility. Additionally, Fourier-transform infrared (FTIR) indices, combined with X-ray diffraction (XRD) and scanning electron microscopy (SEM), provided valuable insights into the physical and chemical degradation of archaeological wood.

Conservation strategies for *Cedrus libani* should include controlled consolidation to prevent further loss of crystallinity, fumigation to inhibit fungal growth and optimized exhibition conditions, including regulated relative humidity, temperature and light intensity, to ensure long-term preservation.

5. Conclusions

This comprehensive, multi-analytical investigation of the wood components of the 4500-year-old Second Solar Boat of Khufu yielded significant insights into ancient Egyptian woodworking practices, degradation mechanisms and conservation challenges. Through the integration of advanced imaging and analytical techniques, wood species were identified, degradation was assessed and fungal biodeteriogens that affected this remarkable archaeological artifact were characterized.

Cedrus libani (Lebanon cedar) is the main wood species used in the construction of the boat, consistent with historical evidence of the import of cedar from Lebanon during the Old Kingdom period for elite boat-building projects, highlighting the sophisticated material selection practices used by the ancient Egyptians. The choice of cedar was likely due to its superior mechanical properties, enhanced durability and hydrophobic characteristics.

Assessment of deterioration revealed complex degradation mechanisms operating at multiple scales. Significant structural changes of the woody cells were evidenced, including their deformation, fracture of the tracheal wall, deterioration of the central lamella and partial structural collapse.

There was evidence of extensive accumulation of soil particles within the woody matrix, which served as catalysts for mechanical, chemical and biological disintegration. Several minerals, such as calcium (Ca), silicon (Si) and sulphur (S), indicated the presence of calcite, gypsum and quartz from the burial environment, which had a significant impact on the mechanical properties, chemical stability and porosity of the wood.

Chemical characterization demonstrated selective molecular disintegration, with indices revealing a high hemicellulose content with relatively low conserved lignin. The high lignin index (4.040) suggests an oxidative breakdown of the aromatic rings of lignin rather than a complete loss. The carbohydrate to lignin ratio (7.656) confirmed the degradation pattern, indicating a loss of carbohydrate to lignin. The low crystallinity index (1.019), corroborated by the crystallinity index (13%), indicates substantial degradation of the crystalline regions of cellulose, resulting in reduced mechanical strength, increased brittleness and altered dimensional stability. Future research should focus on developing conservation protocols specific to cedar wood from arid archaeological contexts, taking into account the unique degradation patterns identified in this study.

Among the fungal species isolated from the deteriorated wooden artifacts, *Aspergillus* (68%) and *Penicillium* (32%) were the predominant genera. Molecular analysis confirmed the identity of the most active cellulolytic species as *Aspergillus flavus* and *Aspergillus terreus*. These fungal species probably employed complex enzymatic processes, including the action of carbohydrate-active enzymes (CAZymes) and reactive oxygen species (ROS), which accelerated the breakdown of wood components and induced oxidative changes. Further investigation into the enzymatic mechanisms employed by the identified fungal species could provide new insights into biodeterioration processes and potential mitigation strategies.

The burial environment was found to be not only a passive factor but also an active player in the degradation process. Mineral deposits in the burial chamber acted as key

catalysts in the systematic dismantling of the structural and molecular composition of wood through the physical disruption of cellular structures, initiation of chemical reactions and modification of internal conditions.

Overall, these results provide valuable insights into the long-term degradation processes of archaeological wood in arid environments and enhance our understanding of ancient Egyptian woodworking practices. The multi-analytical approach used in this study provides a comprehensive framework for assessing the conservation status of similar wooden artifacts and can inform future conservation strategies. The results underscore the importance of considering the complex interplay of physical, chemical and biological factors in the deterioration of archaeological wood and highlight the need for customized conservation approaches that address these multifaceted deterioration mechanisms.

Author Contributions: Writing original draft, S.I. and D.M.A.; Writing-review and editing, S.I., P.G. and D.M.A.; Conceptualization and methodology, S.I. and D.M.A.; Data curation, S.I., P.G. and D.M.A.; Supervision; S.I., P.G. and D.M.A.; Project administration, P.G.; Formal analysis and investigation, L.M., M.V., H.M.K.A.-F. and A.R. All authors have read and agreed to the published version of the manuscript.

Funding: Financial and technical support by the International Atomic Energy Agency (IAEA) under the coordinated research project titled by "Development and Implementation of Cultural Heritage Preservation using Ionizing Radiation Technology", CRP Code: (F22082), contract no. (26680), Contract title: "Studying the Effects of Ionizing Irradiation for Disinfection and Consolidation Purpose of Cellulosic Egyptian Cultural Heritage". The International Centre for Theoretical Physics (ICTP) also provide a financial support under the ICTP-Elettra Users Programme for access to Elettra Sincrotrone Trieste MCX beamline (proposal No. 20200010).

Institutional Review Board Statement: Not applicable.

Informed Consent Statement: Not applicable.

Data Availability Statement: The raw data supporting the conclusions of this article will be madeavailable by the authors on re-quest.

Acknowledgments: The authors acknowledge Anna Fedrigo, beamline scientist at ILL facility (Grenoble, France), who supported us in the synchrotron-based computed tomography experiments.

Conflicts of Interest: The authors declare no conflicts of interest.

References

1. Gale, R.; Gasson, P.; Hepper, N.; Killen, G. Wood. In *Ancient Egyptian Materials and Technology*; Nicholson, P.T., Shaw, I., Eds.; Cambridge University Press: Cambridge, UK, 2000; pp. 334–371.
2. Kim, Y.; Singh, A.P. Wood as Cultural Heritage Material and its Deterioration by Biotic and Abiotic Agents. In *Secondary Xylem Biology*; Elsevier: Amsterdam, The Netherlands, 2016; pp. 233–257.
3. Jenkins, N. *The Boat Beneath The Pyramid. King Cheops' Royal Ship*; Holt Rinehart & Winston: New York, NY, USA, 1980.
4. Mark, S. The Abydos BG 10 Boat and Implications for Standardisation, Innovation, and Timber Conservation in Early Dynastic Boat-Building. *J. Egypt. Archaeol.* **2012**, *98*, 107–126. [CrossRef]
5. Moustafa, A.Y.; Osman, M.S.; Nour, M.Z.; Iskander, Z. *The Cheops Boats*; General Organization for Government Printing Offices: Cairo, Egypt, 1960.
6. Morabito, M.G.; Brier, B.; Greene, S. Preliminary Stability and Resistance Analysis of the Cheops Boat. *J. Sh. Prod. Des.* **2020**, *36*, 14–40. [CrossRef]
7. Landström, B. *Ships of the Pharaohs; 4000 Years of Egyptian Shipbuilding*; Doubleday: Garden City, NY, USA, 1970; ISBN 978-0385078306.
8. Vinson, S. Transportation. In *UCLA Encyclopedia of Egyptology*; Wendrich, W., Dieleman, J., Frood, E., Baines, J., Eds.; University of California: Los Angeles, CA, USA, 2013.
9. Van de Moortel, A. *Sacred and Secular: Ancient Egyptian Ships and Boats*; Archaeological Institute of America Monographs: Philadelphia, PA, USA; University of Pennsylvania Museum: Philadelphia, PA, USA, 2000; ISBN 0-7872-7182-9.
10. Creasman, P.P. Ship Timber and the Reuse of Wood in Ancient Egypt. *J. Egypt Hist.* **2013**, *6*, 152–176. [CrossRef]

11. Bui, H. Density Images by Microgravity. In *Imaging the Cheops Pyramid. Solid Mechanics and Its Applications*; Springer: Dordrecht, The Netherlands, 2012; Volume 182. [CrossRef]
12. Yoshimura, K. A Comparative Study Between Khufu's First and Second Boats in Respect of Their Materials, Archaeological Conditions, and Conservation. Master's Thesis, American University in Cairo, AUC Knowledge Fountain, Cairo, Egypt, 2024.
13. Arranz-Otaegui, A. Evaluating the impact of water flotation and the state of the wood in archaeological wood charcoal remains: Implications for the reconstruction of past vegetation and identification of firewood gathering strategies at Tell Qarassa North (south Syria). *Quat. Int.* **2017**, *457*, 60–73. [CrossRef]
14. Mohamed, S.; Abdel-Fatah, M.A.; Mohamed, W.S.; Omar, A.M.; Waly, N.; Hamdy, R. Conservation of A Painted Wooden Coffin at Dahshur Archaeological Area. *Int. J. Conserv. Sci.* **2024**, *15*, 391–402. [CrossRef]
15. Łucejko, J.J.; Modugno, F.; Ribechini, E.; Tamburini, D.; Colombini, M.P. Analytical Instrumental Techniques to Study Archaeological Wood Degradation. *Appl. Spectrosc. Rev.* **2015**, *50*, 584–625. [CrossRef]
16. Atwa, D.M.; Ibrahim, S.; Stani, C.; Birarda, G.; Ali, N.; Abdullah, E.; Vaccari, L.; Grenni, P.; Visca, A.; Badr, Y.; et al. Biodeterioration Assessment of a Unique Old Pharaonic Kingdom Wooden Statue Using Advanced Diagnostic Techniques. *Appl. Sci.* **2022**, *12*, 7020. [CrossRef]
17. Chu, S.; Lin, L.; Zhang, Y.; Wang, D. Physicochemical structure and micromechanical properties of archaeological wood under alternating dry and wet conditions. *Wood Mater. Sci. Eng.* **2024**, *19*, 691–701. [CrossRef]
18. Szwajca, A.; Lucejko, J.J.; Berdychowska, N.; Zborowska, M. Understanding changes in holocellulose and lignin compounds in wooden structure of veneers: Molecular insights post hydrothermal treatment and aging. *Int. J. Biol. Macromol.* **2024**, *266*, 130920. [CrossRef]
19. Han, L.; Xi, G.; Dai, W.; Zhou, Q.; Sun, S.; Han, X.; Guo, H. Influence of Natural Aging on the Moisture Sorption Behaviour of Wooden Structural Components. *Molecules* **2023**, *28*, 1946. [CrossRef]
20. Wang, B.; Qi, M.; Ma, Y.; Zhang, B.; Hu, Y. Microbiome Diversity and Cellulose Decomposition Processes by Microorganisms on the Ancient Wooden Seawall of Qiantang River of Hangzhou, China. *Microb. Ecol.* **2023**, *86*, 2109–2119. [CrossRef] [PubMed]
21. Wang, H.; Feyereisen, G.W.; Zhang, J.; Ishii, S. Fungal degradation of complex organic carbon supports denitrification in saturated woodchip bioreactors. *Bioresour. Technol.* **2025**, *417*, 131826. [CrossRef]
22. Stelzner, I.; Stelzner, J.; Gwerder, D.; Martinez-Garcia, J.; Schuetz, P. Imaging and Assessment of the Microstructure of Conserved Archaeological Pine. *Forests* **2023**, *14*, 211. [CrossRef]
23. Bouramdane, Y.; Haddad, M.; Mazar, A.; Aît Lyazidi, S.; Oudghiri Hassani, H.; Boukir, A. Aged Lignocellulose Fibers of Cedar Wood (9th and 12th Century): Structural Investigation Using FTIR-Deconvolution Spectroscopy, X-Ray Diffraction (XRD), Crystallinity Indices, and Morphological SEM Analyses. *Polymers* **2024**, *16*, 3334. [CrossRef]
24. Abdel-Azeem, A.M.; Held, B.W.; Richards, J.E.; Davis, S.L.; Blanchette, R.A. Assessment of biodegradation in ancient archaeological wood from the Middle Cemetery at Abydos, Egypt. *PLoS ONE* **2019**, *14*, e0213753. [CrossRef]
25. Blanchette, R.A.; Haight, J.E.; Koestler, R.J.; Hatchfield, P.B.; Arnold, D. Assessment of Deterioration in Archaeological Wood from Ancient Egypt. *J. Am. Inst. Conserv.* **1994**, *33*, 55. [CrossRef]
26. Watt, D.; Colston, B. Investigating the effects of humidity and salt crystallisation on medieval masonry. *Build. Environ.* **2000**, *35*, 737–749. [CrossRef]
27. Branca, C.; Albano, A.; Di Blasi, C. Critical evaluation of global mechanisms of wood devolatilization. *Thermochim. Acta* **2005**, *429*, 133–141. [CrossRef]
28. Geweely, N.; Abu Taleb, A.; Ibrahim, S.; Grenni, P.; Caneva, G.; Galotta, G.; Abdallah, M.; Atwa, D.; Plaisier, J.; Antonelli, F. New data on relevant ancient Egyptian wooden artifacts: Identification of wooden species and study of the state of conservation with multidisciplinary analyses. *Archaeometry* **2023**, *65*, 165–183. [CrossRef]
29. Yang, W.; Ma, W.; Liu, X. Evaluation of Deterioration Degree of Archaeological Wood from Luoyang Canal No. 1 Ancient Ship. *Forests* **2024**, *15*, 963. [CrossRef]
30. Abdrabou, A.; Hussein, A.; Sultan, G.M.; Kamal, H.M. New insights into a polychrome Middle Kingdom palette applied to a wooden coffin: A multidisciplinary analytical approach. *J. Cult. Herit.* **2022**, *54*, 118–129. [CrossRef]
31. Vigorelli, L.; Re, A.; Giudorzi, L.; Cavaleri, T.; Buscaglia, P.; Nervo, M.; Del Vesco, P.; Borla, M.; Grassini, S.; Lo Giudice, A. Multi-analytical approach for the study of an ancient Egyptian wooden statuette from the collection of Museo Egizio of Torino. *Acta Imeko* **2022**, *11*, 10. [CrossRef]
32. Afifi, H.A.M.; Basta, S.A.; Mostafa, A.M. Examination and analysis of a stored stucco window in the conservation lab of Bab Al-azab area, citadel of Salah Al-din Al-Ayyubi, Cairo Egypt. *Radiat. Phys. Chem.* **2024**, *218*, 111627. [CrossRef]
33. Balzano, A.; Merela, M.; Čufar, K. Scanning Electron Microscopy Protocol for Studying Anatomy of Highly Degraded Waterlogged Archaeological Wood. *Forests* **2022**, *13*, 161. [CrossRef]
34. Tamburini, D.; Łucejko, J.J.; Pizzo, B.; Mohammed, M.Y.; Sloggett, R.; Colombini, M.P. A critical evaluation of the degradation state of dry archaeological wood from Egypt by SEM, ATR-FTIR, wet chemical analysis and Py(HMDS)-GC-MS. *Polym. Degrad. Stab.* **2017**, *146*, 140–154. [CrossRef]

35. Traoré, M.; Kaal, J.; Martínez Cortizas, A. Application of FTIR spectroscopy to the characterization of archeological wood. *Spectrochim. Acta Part A Mol. Biomol. Spectrosc.* **2016**, *153*, 63–70. [CrossRef]
36. Afifi, H.A.M.; Mansour, M.M.A.; Hassan, A.G.A.I.; Salem, M.Z.M. Biodeterioration effects of three Aspergillus species on stucco supported on a wooden panel modeled from Sultan al-Ashraf Qaytbay Mausoleum, Egypt. *Sci. Rep.* **2023**, *13*, 15241. [CrossRef]
37. Geweely, N.S.; Abu Taleb, A.M.; Grenni, P.; Caneva, G.; Atwa, D.M.; Plaisier, J.R.; Ibrahim, S. Eco-Friendly Preservation of Pharaonic Wooden Artifacts using Natural Green Products. *Appl. Sci.* **2024**, *14*, 5023. [CrossRef]
38. Andonova, M. Ancient basketry on the inside: X-ray computed microtomography for the non-destructive assessment of small archaeological monocotyledonous fragments: Examples from Southeast Europe. *Herit. Sci.* **2021**, *9*, 158. [CrossRef]
39. Stelzner, J.; Million, S. X-ray Computed Tomography for the anatomical and dendrochronological analysis of archaeological wood. *J. Archaeol. Sci.* **2015**, *55*, 188–196. [CrossRef]
40. Sodini, N.; Dreossi, D.; Giordano, A.; Kaiser, J.; Zanini, F.; Zikmund, T. Comparison of different experimental approaches in the tomographic analysis of ancient violins. *J. Cult. Herit.* **2017**, *27*, S88–S92. [CrossRef]
41. Dreossi, D.; Sodini, N.; Zanini, F. Synchrotron Radiation Microtomography: A Tool for the Non-Invasive Structural Analysis of Historical Musical Instruments. *Synchrotron Radiat. News* **2019**, *32*, 17–21. [CrossRef]
42. Bentivoglio-Ravasio, B.; Marconi, E.; Trotta, L.; Dreossi, D.; Sodini, N.; Mancini, L.; Zanini, F.; Tonini, C. Synchrotron radiation microtomography of musical instruments: A non-destructive monitoring technique for insect infestations. *J. Entomol. Acarol. Res.* **2011**, *43*, 149. [CrossRef]
43. Whitau, R.; Dilkes-Hall, I.E.; Dotte-Sarout, E.; Langley, M.C.; Balme, J.; O'Connor, S. X-ray computed microtomography and the identification of wood taxa selected for archaeological artefact manufacture: Rare examples from Australian contexts. *J. Archaeol. Sci. Rep.* **2016**, *6*, 536–546. [CrossRef]
44. Skóra, J.; Gutarowska, B.; Pielech-Przybylska, K.; Stępień, Ł.; Pietrzak, K.; Piotrowska, M.; Pietrowski, P. Assessment of microbiological contamination in the work environments of museums, archives and libraries. *Aerobiologia* **2015**, *31*, 389–401. [CrossRef] [PubMed]
45. Yoon, J.H.; Park, J.E.; Suh, D.Y.; Hong, S.B.; Ko, S.J.; Kim, S.H. Comparison of Dyes for Easy Detection of Extracellular Cellulases in Fungi. *Mycobiology* **2007**, *35*, 21. [CrossRef]
46. Lu, Y.; Jiao, L.; Sun, G.; Wang, J.; Liu, S.; Li, R.; Zhang, Y.; Guo, Y.; Guo, J.; Jiang, X.; et al. Preservation status and microbial community of waterlogged archaeological woods over 7800 years old at the Jingtoushan Site, China. *Wood Sci. Technol.* **2023**, *57*, 537–556. [CrossRef]
47. Abdrabou, A.; Zidan, E.; Nishisaka, A.; Kurokochi, H.; Yoshimura, S. King Khufu's Second Boat: Scientific Identification of Wood Species for Deckhouse, Canopy, and Forecastle. *Forests* **2022**, *13*, 2118. [CrossRef]
48. Abdrab, A. Scientific Species Identification for the Deckhouse, Canopy and Forecastle of King Khufu's Second Boat. *Arts Soc. Sci. J.* **2022**, *13*, 546. [CrossRef]
49. Giachi, G.; Guidotti, M.C.; Lazzeri, S.; Macchioni, N.; Sozzi, L. Wood identification of some coffins from the Necropolis of Thebes held in the collection of the Egyptian Museum in Florence. *J. Cult. Herit.* **2021**, *47*, 34–42. [CrossRef]
50. Longo, E.; Contillo, A.; D'Amico, L.; Prašek, M.; Saccomano, G.; Sodini, N.; Dullin, C.; Dreossi, D.; Tromba, G. SYRMEP beamline: State of the art, upgrades and future prospects. *Eur. Phys. J. Plus* **2024**, *139*, 880. [CrossRef]
51. Cloetens, P.; Pateyron-Salomé, M.; Buffière, J.Y.; Peix, G.; Baruchel, J.; Peyrin, F.; Schlenker, M. Observation of microstructure and damage in materials by phase sensitive radiography and tomography. *J. Appl. Phys.* **1997**, *81*, 5878–5886. [CrossRef]
52. Paganin, D.; Mayo, S.C.; Gureyev, T.E.; Miller, P.R.; Wilkins, S.W. Simultaneous phase and amplitude extraction from a single defocused image of a homogeneous object. *J. Microsc.* **2002**, *206*, 33–40. [CrossRef]
53. Brun, F.; Pacilè, S.; Accardo, A.; Kourousias, G.; Dreossi, D.; Mancini, L.; Tromba, G.; Pugliese, R. Enhanced and Flexible Software Tools for X-ray Computed Tomography at the Italian Synchrotron Radiation Facility Elettra. *Fundam. Informaticae* **2015**, *141*, 233–243. [CrossRef]
54. Schneider, C.A.; Rasband, W.S.; Eliceiri, K.W. NIH Image to ImageJ: 25 years of image analysis. *Nat. Methods* **2012**, *9*, 671–675. [CrossRef] [PubMed]
55. Long, K.; Chen, K.; Lin, L.; Fu, F.; Zhong, Y. Deterioration of Microstructures and Properties in Ancient Architectural Wood from Yingxian Wooden Pagoda (1056 AD) during Natural Aging. *Forests* **2023**, *14*, 393. [CrossRef]
56. Rebuffi, L.; Plaisier, J.R.; Abdellatief, M.; Lausi, A.; Scardi, P. MCX: A Synchrotron Radiation Beamline for X-ray Diffraction Line Profile Analysis. *Zeitschrift für Anorg. und Allg. Chemie* **2014**, *640*, 3100–3106. [CrossRef]
57. Plaisier, J.R.; Nodari, L.; Gigli, L.; Rebollo San Miguel, E.P.; Bertoncello, R.; Lausi, A. The X-ray diffraction beamline MCX at Elettra: A case study of non-destructive analysis on stained glass. *Acta Imeko* **2017**, *6*, 71. [CrossRef]
58. Segal, L.; Creely, J.; Martin, A.; Conrad, C. An Empirical Method for Estimating the Degree of Crystallinity of Native Cellulose Using the X-Ray Diffractometer. *Text. Res. J.* **1959**, *29*, 786–794. [CrossRef]
59. Faix, O. Classification of Lignins from Different Botanical Origins by FT-IR Spectroscopy. *Holzforschung* **1991**, *45*, 21–28. [CrossRef]

60. Pandey, K.; Pitman, A. FTIR studies of the changes in wood chemistry following decay by brown-rot and white-rot fungi. *Int. Biodeterior. Biodegrad.* **2003**, *52*, 151–160. [CrossRef]
61. Darwish, S.; El Hadidi, N.M.N.; Mansour, M. The Effect of Fungal Decay on Ficus Sycomorus Wood. *Int. J. Conserv. Sci.* **2013**, *4*, 271–282.
62. Cavallaro, G.; Agliolo Gallitto, A.; Lisuzzo, L.; Lazzara, G. Comparative study of historical woods from XIX century by thermogravimetry coupled with FTIR spectroscopy. *Cellulose* **2019**, *26*, 8853–8865. [CrossRef]
63. Andersson, S.; Serimaa, R.; Paakkari, T.; SaranpÄÄ, P.; Pesonen, E. Crystallinity of wood and the size of cellulose crystallites in Norway spruce (*Picea abies*). *J. Wood Sci.* **2003**, *49*, 531–537. [CrossRef]
64. Guo, J.; Xiao, L.; Han, L.; Wu, H.; Yang, T.; Wu, S.; Yin, Y. Deterioration of the cell wall in waterlogged wooden archeological artifacts, 2400 years old. *IAWA J.* **2019**, *40*, 820–844. [CrossRef]
65. Pozhidaev, V.M.; Retivov, V.M.; Panarina, E.I.; Sergeeva, Y.E.; Zhdanovich, O.A.; Yatsishina, E.B. Development of a Method for Identifying Wood Species in Archaeological Materials by IR Spectroscopy. *J. Anal. Chem.* **2019**, *74*, 1192–1201. [CrossRef]
66. Lucejko, J.J.; Tamburini, D.; Zborowska, M.; Babiński, L.; Modugno, F.; Colombini, M.P. Oak wood degradation processes induced by the burial environment in the archaeological site of Biskupin (Poland). *Herit. Sci.* **2020**, *8*, 44. [CrossRef]
67. Kruer-Zerhusen, N.; Cantero-Tubilla, B.; Wilson, D.B. Characterization of cellulose crystallinity after enzymatic treatment using Fourier transform infrared spectroscopy (FTIR). *Cellulose* **2018**, *25*, 37–48. [CrossRef]
68. Raper, K.B.; Thom, C.; Fennell, D.I. *A Manual of the Penicillia*; Williams & Wilkins: Baltimore, MD, USA, 1949.
69. Raper, K.; Fennell, D. *The Genus Aspergillus*; Krieger Publishing Company, Huntington: New York, NY, USA, 1977.
70. Tamura, K.; Stecher, G.; Peterson, D.; Filipski, A.; Kumar, S. MEGA6: Molecular Evolutionary Genetics Analysis Version 6.0. *Mol. Biol. Evol.* **2013**, *30*, 2725–2729. [CrossRef]
71. Raper, K.; Fennell, D. *The Genus Aspergillus*; Williams and Wilkins Company: Philadelphia, PA, USA, 1965.
72. Gilman, J.C. *A Manual of Soil Fungi*; Biotech Books: New Delhi, India, 1977; ISBN 8176220116.
73. Samson, R.A.; Pitt, J.I. The Genus Penicillium and Its Teleomorphic States Eupenicillium and Talaromyces. *Mycologia* **1981**, *73*, 582. [CrossRef]
74. El-Shafie, A.K. Soil fungi in Qatar and other Arab countries. *Econ. Bot.* **1996**, *50*, 242. [CrossRef]
75. Kern, M.E.; Blevins, K.S. Laboratory procedures for fungal culture and isolation. In *Medical Mycology: A Self-Instructional Text*; FA Davis Company: Philadelphia, PA, USA, 1997; pp. 27–72.
76. Domsch, K.H.; Gams, W.; Anderson, T.H. *Compendium of Soil Fungi*, 2nd ed.; Academic Press: London, UK, 2007.
77. Klich, M.A. *Identification of Common Aspergillus Species*; Centraal Bureau Voor Schim: Utrecht, The Netherlands, 2002.
78. Kwiatkowska, M.; Ważny, R.; Turnau, K.; Wójcik, A. Fungi as deterioration agents of historic glass plate negatives of Brandys family collection. *Int. Biodeterior. Biodegrad.* **2016**, *115*, 133–140. [CrossRef]
79. White, T.J.; Bruns, T.; Lee, S.; Taylor, J. Amplification and direct sequencing of fungal ribosomal RNA genes for phylogenetics. In *PCR Protocols*; Elsevier: Amsterdam, The Netherlands, 1990; pp. 315–322.
80. Yaman, B. Anatomy of Lebanon cedar (*Cedrus libani* A. Rich.) wood with indented growth rings. *Acta Biol. Cracoviensia* **2007**, *49*, 19–23.
81. Arbuckle MacLeod, C. Lebanese Cedar, Skeuomorphs, Coffins, and Status in Ancient Egypt. *Arts* **2024**, *13*, 163. [CrossRef]
82. Wilkinson, T. *The Thames & Hudson Dictionary of Ancient Egypt*; Thames & Hudson: London, UK, 2005; ISBN 9780500051375.
83. Broda, M.; Popescu, C.-M.; Curling, S.F.; Timpu, D.I.; Ormondroyd, G.A. Effects of Biological and Chemical Degradation on the Properties of Scots Pine Wood—Part I: Chemical Composition and Microstructure of the Cell Wall. *Materials* **2022**, *15*, 2348. [CrossRef]
84. Ojeda-Magaña, B.; Ruelas, R.; Quintanilla-Domínguez, J.; Robledo-Hernández, J.G.; Sturrock, C.J.; Mooney, S.J.; Tarquis, A.M. Detection and quantification of pore, solid and gravel spaces in CT images of a 3D soil sample. *Appl. Math. Model.* **2020**, *85*, 360–377. [CrossRef]
85. Bouramdane, Y.; Fellak, S.; El Mansouri, F.; Boukir, A. Impact of Natural Degradation on the Aged Lignocellulose Fibers of Moroccan Cedar Softwood: Structural Elucidation by Infrared Spectroscopy (ATR-FTIR) and X-ray Diffraction (XRD). *Fermentation* **2022**, *8*, 698. [CrossRef]
86. Wang, B.; Zhu, C.; Wang, B.; Zhang, B.; Hu, Y. Analysis of the biocorrosion community from ancient wooden constructions at Tianluoshan (7000–6300 cal BP), Zhejiang Province, China. *Herit. Sci.* **2024**, *12*, 189. [CrossRef]
87. Molinelli, L.; Drula, E.; Gaillard, J.-C.; Navarro, D.; Armengaud, J.; Berrin, J.-G.; Tron, T.; Tarrago, L. Methionine oxidation of carbohydrate-active enzymes during white-rot wood decay. *Appl. Environ. Microbiol.* **2024**, *90*, e01931-23. [CrossRef]
88. Zalamea, M.; González, G.; Lodge, D. Physical, Chemical, and Biological Properties of Soil under Decaying Wood in a Tropical Wet Forest in Puerto Rico. *Forests* **2016**, *7*, 168. [CrossRef]
89. Miliša, M.; Belančić, A.; Kepčija, R.M.; Sertić-Perić, M.; Ostojić, A.; Habdija, I. Calcite deposition in karst waters is promoted by leaf litter breakdown and vice versa. *Ann. Limnol.—Int. J. Limnol.* **2010**, *46*, 225–232. [CrossRef]

90. Klaassen, R.; van 't Oor, M.; Kloppenburg, A.; Huisman, H. Rate of occurrence of wood degradation in foundations and archaeological sites when groundwater levels are too low. *J. Cult. Herit.* **2023**, *63*, 23–31. [CrossRef]
91. Abdel Moneim, A.A. Overview of the geomorphological and hydrogeological characteristics of the Eastern Desert of Egypt. *Hydrogeol. J.* **2005**, *13*, 416–425. [CrossRef]
92. Raynaud, S.; de La Boisse, H.; Makroum, F.M.; Bertho, J. Geological and topographical study of the original hills at the base of Fourth Dynasty Egyptian monuments of the Memphite plateau. *Bull. la Société Géologique Fr.* **2010**, *181*, 279–290. [CrossRef]
93. Popescu, C.M.; Vasile, C.; Popescu, C.; Singurel, G. Degradation of Lime Wood Painting Supports II. Spectral Characterisation. *Cellul. Chem. Technol.* **2006**, *40*, 649–658.
94. Zhou, Y.; Matsui, T.; Liu, C.; Wang, F. Degradation Phenomena of Wooden Pillars in the Main Hall of the Fengguo Monastery, Yixian, Liaoning, China—Scientific Investigation with XRD, IC, and FTIR Analysis. *J. Conserv. Sci.* **2020**, *36*, 15–27. [CrossRef]
95. Moosavinejad, S.M.; Madhoushi, M.; Vakili, M.; Rasouli, D. Evaluation of degradation in chemical compounds of wood in historical buildings using FT-IR and FT-Raman vibrational spectroscopy. *Maderas. Cienc. y Tecnol.* **2019**, *21*, 381–392. [CrossRef]
96. Emmanuel, V.; Odile, B.; Céline, R. FTIR spectroscopy of woods: A new approach to study the weathering of the carving face of a sculpture. *Spectrochim. Acta Part A Mol. Biomol. Spectrosc.* **2015**, *136*, 1255–1259. [CrossRef]
97. Bock, P.; Gierlinger, N. Infrared and Raman spectra of lignin substructures: Coniferyl alcohol, abietin, and coniferyl aldehyde. *J. Raman Spectrosc.* **2019**, *50*, 778–792. [CrossRef]
98. Wang, S.-N.; Zhang, F.-D.; Huang, A.-M.; Zhou, Q. Distinction of four Dalbergia species by FTIR, 2 nd derivative IR, and 2D-IR spectroscopy of their ethanol-benzene extractives. *Holzforschung* **2016**, *70*, 503–510. [CrossRef]
99. Geminiani, L.; Campione, F.; Corti, C.; Luraschi, M.; Motella, S.; Recchia, S.; Rampazzi, L. Differentiating between Natural and Modified Cellulosic Fibres Using ATR-FTIR Spectroscopy. *Heritage* **2022**, *5*, 4114–4139. [CrossRef]
100. Zhou, G.; Taylor, G.; Polle, A. FTIR-ATR-based prediction and modelling of lignin and energy contents reveals independent intra-specific variation of these traits in bioenergy poplars. *Plant Methods* **2011**, *7*, 9. [CrossRef] [PubMed]
101. Boukir, A.; Fellak, S.; Doumenq, P. Structural characterization of Argania spinosa Moroccan wooden artifacts during natural degradation progress using infrared spectroscopy (ATR-FTIR) and X-Ray diffraction (XRD). *Heliyon* **2019**, *5*, e02477. [CrossRef]
102. Guo, J.; Chen, J.; Meng, Q.; Ploszczanski, L.; Liu, J.; Luo, R.; Jin, T.; Siedlaczek, P.; Lichtenegger, H.C.; Yin, Y.; et al. Molecular and crystal structures of cellulose in severely deteriorated archaeological wood. *Cellulose* **2022**, *29*, 9549–9568. [CrossRef]
103. Kaya, A.I.; Çiftçi, A.; İlkuçar, M. Use of Fourier Transform Infrared Spectroscopy and Artificial Neural Networks to predict the wood density of *Cedrus libani* A. Rich. *Fresenius Environ. Bull.* **2021**, *30*, 3141–3148.
104. Strudwick, N. The Old Kingdom and First Intermediate Period. In *The Oxford Handbook of Egyptology*; Shaw, I., Bloxam, E., Eds.; Oxford University Press: Oxford, UK, 2020; pp. 618–637.
105. Opdenbosch, D. Van Influences on the accuracy of crystallinities determined by the method of Ruland and Vonk. *Cellulose* **2023**, *30*, 4197–4213. [CrossRef]
106. Debnath, A.; Santra, R. Theory of high-energy correlated multiphoton x-ray diffraction for synchrotron-radiation sources. *Phys. Rev. Res.* **2023**, *5*, 023158. [CrossRef]
107. Ren, Y. High-Energy Synchrotron X-Ray Diffraction and Its Application to In Situ Structural Phase-Transition Studies in Complex Sample Environments. *JOM* **2012**, *64*, 140–149. [CrossRef]
108. Ahmad, A.; Elserogy, A.; Al-Muheisen, Z.; Villeneuve, F.; El-Oqlah, A. The conservation of a wooden nabataean coffin box from Jordan-application of non-destructive ultrasonic technique. *Wood Res.* **2018**, *63*, 1–14.
109. Osman, M.E.S.; El-Shaphy, A.A.E.N.; Meligy, D.A.; Ayid, M.M. Survey for fungal decaying archaeological wood and their enzymatic activity. *Int. J. Conserv. Sci.* **2015**, *5*, 295–308.
110. Helmi, F.M.; Ali, S.M.; Ismael, N.M. Nanomaterials for the inhibition of microbial growth on ancient Egyptian funeral masks. *Mediterr. Archaeol. Archaeom.* **2015**, *15*, 87–95. [CrossRef]
111. Tamura, K.; Stecher, G.; Kumar, S. MEGA11: Molecular Evolutionary Genetics Analysis Version 11. *Mol. Biol. Evol.* **2021**, *38*, 3022–3027. [CrossRef] [PubMed]
112. Ortiz-Santana, B.; Lindner, D.L.; Miettinen, O.; Justo, A.; Hibbett, D.S. A phylogenetic overview of the antrodia clade (Basidiomycota, Polyporales). *Mycologia* **2013**, *105*, 1391–1411. [CrossRef] [PubMed]
113. Pedersen, N.B.; Matthiesen, H.; Blanchette, R.A.; Alfredsen, G.; Held, B.W.; Westergaard-Nielsen, A.; Hollesen, J. Fungal attack on archaeological wooden artefacts in the Arctic—Implications in a changing climate. *Sci. Rep.* **2020**, *10*, 14577. [CrossRef]
114. Blanchette, R.A. A review of microbial deterioration found in archaeological wood from different environments. *Int. Biodeterior. Biodegradation* **2000**, *46*, 189–204. [CrossRef]